Synthesis of Well-Defined Microporous Carbons by Molecular-Scale Templating with Polyhedral Oligomeric Silsesquioxane Moieties

Zhenghui Li,[†] Dingcai Wu,*,[†] Yeru Liang,[†] Ruowen Fu,[†] and Krzysztof Matyjaszewski*,[‡]

[†]Materials Science Institute, PCFM Lab and DSAPM Lab, School of Chemistry and Chemical Engineering, Sun Yat-sen University, Guangzhou 510275, P. R. China

[‡]Department of Chemistry, Carnegie Mellon University, 4400 Fifth Avenue, Pittsburgh, Pennsylvania 15213, United States

S *Supporting Information*

ABSTRACT: Formation of a uniform interface between the carbon precursor and the selected template is critical for preparing high-quality nanoporous carbons. It can be accomplished by various templating procedures but still remains a challenge, especially for microporous carbons. A new strategy to fabricate well-defined microporous carbon nanosphere (MCNS) materials via molecular-scale interfacial engineering using an organic/inorganic hybrid molecule as the building block was designed. A commercially available octaphenyl polyhedral oligomeric silsesquioxane was selected as such a building block and transformed into the MCNS products via cross-linking of organic components, followed by carbonization, and subsequent removal of monodispersed silica domains, surrounded by molecular-scale carbon/silica interfaces. The obtained MCNS materials exhibit very large surface area (e.g., 2264 m^2/g) and fast and selective sorption, and thus demonstrate excellent adsorption and supercapacitance properties. These findings could provide a new benchmark for preparing well-defined nanoporous carbons for various applications.

Nanocarbons, including porous carbons, carbon nanotubes, graphenes, and fullerenes, form a class of innovative advanced materials that find utility in multiple applications related to energy,[1] environment,[2] electronics,[3] magnetics,[4] medicine,[5] sensors,[6] catalysis,[7] etc. Porous carbons have attracted increasing attention because of their large surface area, large pore volume, good conductivity, and high chemical and physical stability.[8] Due to the decisive role of the nanostructure of the porous carbons in determining the material performance in the targeted application, the past decades have witnessed the generation of a spectrum of novel nanoporous carbons with various well-defined nanostructures, including ordered/disordered mesoporous carbons,[9] ordered/disordered macroporous carbons,[10] hollow carbon nanospheres,[11] and hierarchical porous carbons.[12]

Most of these nanoporous carbons are fabricated by templating methods.[13] However, since the templates and carbon sources are usually two incompatible materials,[14] a non-uniform interface is often formed between the template and carbon source during the tedious molding/casting procedures for the hard-templating processes or the complicated microphase separation procedures for the soft-templating methods.[15] This
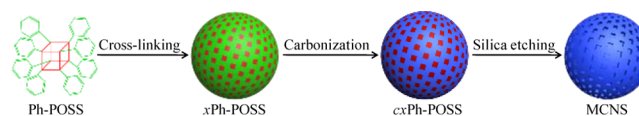
Figure 1. Schematic illustration of preparation of MCNS materials.

inevitably leads to many serious limitations, including formation of nonporous carbon by-products and ill-defined pore structure defects, because there exist deposition of carbon sources on the external surface of hard templates, incomplete filling of carbon sources in the pores of hard templates, and weak interaction between carbon sources and soft templates.[15] Thus, it remains a great challenge to form a highly uniform interface between the templates and carbon sources when adopting macroscopic templating methods to fabricate well-defined porous carbons.

Here we report development of a remarkably precise concept of molecular-scale interface engineering to design and fabricate well-defined microporous carbon nanospheres (MCNSs). Key to this novel preparation strategy is a new organic/inorganic hybrid building block. The building block selected to demonstrate this procedure is a commercially available octaphenyl polyhedral oligomeric silsesquioxane (Ph-POSS, Figures 1 and S1). The phenyl groups in Ph-POSS are cross-linked in solution to form a macroscopic polymer network, forming an extended polymeric/inorganic hybrid material. The formed xPh-POSS particles provide a uniform carbon source/template interface on the molecular scale. Interestingly, because of the cross-linking-induced phase separation, xPh-POSS provides a uniform nanosphere morphology. Thus, a novel class of MCNSs can be generated by carbonization of the xPh-POSS nanospheres, followed by removal of silica domains in the resulting carbonized xPh-POSS (cxPh-POSS).

The silica domains are monodispersed in cxPh-POSS because of the robust covalent molecular-scale carbon/silica interface. To our knowledge, the formed microporous carbons have the smallest pore size (1.3 nm) when compared to all previous reports of using silica templates to prepare conventional porous carbons, thus providing an intriguing example of the use of structured silica templates for synthesis of microporous carbons. The as-prepared MCNS materials demonstrate very large surface area, uniform templated micropores, and high micropore ratio, and exhibit excellent adsorption and supercapacitance properties.

Since POSS is a widely used filler to enhance the thermal stability and mechanical properties of polymeric materials,[16] it is commercially available and inexpensive. Nevertheless, use of this low-cost organic/inorganic hybrid molecule as a raw material for synthesis of porous carbons has not been reported, most likely due to its decomposition at the high temperatures required for carbonization. To address this issue, a simple Friedel−Crafts cross-linking reaction was employed with the Ph-POSS molecules over a 12 h period to form xPh-POSS. During this treatment, both intra- and intermolecular cross-linking of the phenyl groups in Ph-POSS molecules occurred, forming a 3D continuous network. The obtained polymeric/inorganic hybrid material xPh-POSS displayed a high weight gain of 43%, attributed to introduction of abundant -CO- cross-linking bridges (Figures S2 and S3) and possible Cl-containing groups from side reactions (Figures S4 and S5), indicating a highly cross-linked structure. The weight percentages of polymeric and inorganic components for xPh-POSS are calculated to be 72% and 28%, respectively, consistent with TGA results of xPh-POSS under air (75% and 25%, respectively; Figure S6).

The pyrolysis yield after carbonization of xPh-POSS at 900 °C was 69%, according to TGA under N_2 (Figure S6), which could be translated into a carbonization yield of the polymeric xPh of 57%. This indicates that xPh-POSS, formed by cross-linking Ph-POSS building blocks, is a perfect material for synthesis of porous carbons, since it simultaneously contains a carbon source and a well-defined hard template and thus can avoid the tedious casting and hard-to-handle interface engineering control procedures utilized for conventional hard-templating methods.

The xPh-POSS formed during the solution-based cross-linking reaction provides a spherical nanomorphology with an average diameter of 360 nm (Figures 2A and S7). Because of the nature of the rigid polymeric network, this spherical nano-morphology can be retained during carbonization at 900 °C with a heating rate of 5 °C/min (Figure 2B). Moreover, this carbonization treatment does not lead to any silica agglomeration (Figure 2C), and thus Si and O elements of the silica template are distributed very homogeneously within the carbon framework after carbonization, according to EELS mapping images of C, Si, and O elements for the as-obtained cxPh-POSS-900-5 (Figure
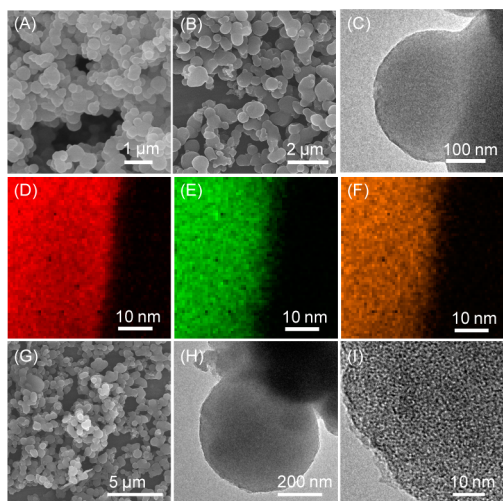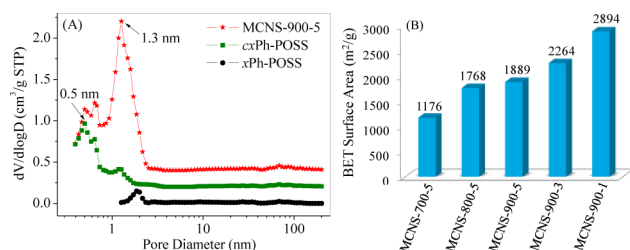
Figure 3. (A) DFT pore size distributions of xPh-POSS, cxPh-POSS-900-5, and MCNS-900-5. (B) BET surface areas of MCNSs obtained at various carbonization temperatures and heating rates.

2D−F). This indicates that the unique molecular-scale carbon/silica interface of xPh-POSS can effectively act as a barrier against silica fusion during the high-temperature carbonization.

After carbonization, the resulting carbon framework demonstrates a graphite-like microcrystalline structure, whose carbon sheets and clusters have a microcrystalline plane crystal size of 1.2 nm (Figure S8 and Table S1) and form many micropores with a maximum pore size distribution peak at 0.5 nm (Figures 3A and S9) because of their disordered packing. Thus, HF can enter into the carbon framework through these micropores and etch the uniformly distributed silica domains in cxPh-POSS-900-5 to generate well-defined silica-templated micropores of 1.3 nm diameter (Figures 3A and S9), very close to the size of the POSS core of the Ph-POSS building block (1 nm, Figure S1), forming the microporous carbon nanosphere product MCNS-900-5 with an average nanosphere diameter of 330 nm (Figures 2G−I and S10). This class of 1.3 nm-sized micropores are the smallest silica-templated nanopores reported to date (normally >2 nm, Table S2), which can be attributed to one advantage of the as-developed effective molecular-scale interface engineering.

A Brunauer−Emmett−Teller (BET) calculation reveals that MCNS-900-5 has a BET surface area (S_{BET}) of up to 1889 m^2/g (Figure S11). The t-plot method gives a micropore surface area (S_{mic}) for MCNS-900-5 equal to 1779 m^2/g, indicating a very high micropore ratio of 94% (S_{mic}/S_{BET}, Table S3), much higher than those for most conventional templated microporous carbons and activated carbons (normally 35−85%).[17]

Furthermore, the pore structure of this class of MCNSs can be easily tuned by controlling the carbonization conditions for the xPh-POSS. Both increasing the carbonization temperature and decreasing the heating rate led to a decrease in the carbonization yield for the xPh component of the xPh-POSS and thus an increase in the silica/carbon ratio of the resulting cxPh-POSS products (Table S4), which enhanced the microporosity after removal of the silica templates. For example, S_{BET} increased from 1176 to 1889 m^2/g when the carbonization temperature was increased from 700 to 900 °C at a heating rate of 5 °C/min, and further increased to 2264 m^2/g when the heating rate was reduced to 3 °C/min at the carbonization temperature of 900 °C (Figures 3B, S12, and S13 and Table S3). This very high surface area for the as-prepared MCNS-900-3 is much greater than those for most carbon particles without activation and is even comparable to those of many activated carbon spheres which were obtained through complicated activation procedures in a very low yield (Table S5). It should be noted that an extended carbonization treatment with a very slow heating rate of 1 °C/min caused a slight degree of silica agglomeration, forming some silica-templated mesopores, resulting in bimodal pore size distributions at 1.3 and 2.0 nm (Figure S14), despite achieving

Figure 2. (A) SEM image xPh-POSS. (B) SEM and (C)TEM images of cxPh-POSS-900-5. EELS mapping images of (D) carbon, (E) silicon, and (F) oxygen for cxPh-POSS-900-5. (G) SEM and (H,I) TEM images of MCNS-900-5.

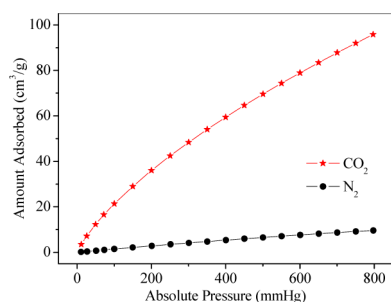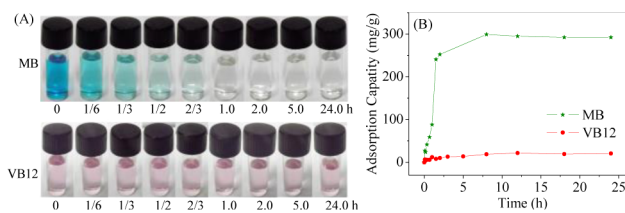**Figure 4.** CO_2 and N_2 adsorption isotherms at 0 °C for MCNS-900-5.

Figure 6. (A) Galvanostatic charge/discharge curves of MCNS-900-3 and MCNS-900-5 at a current density of 200 mA/g. (B) Mass-specific capacitances at various current densities for MCNS-900-3 and MCNS-900-5.

an ultrahigh S_{BET} = 2894 m^2/g for the resulting MCNS-900-1 product (Figure S15 and Table S3).

The adsorption and supercapacitance performances of these unique MCNS materials were studied. CO_2 is the major anthropogenic greenhouse gas, and its excessive emission has been deemed one of the most important causes of global warming.[18] Thus, the development of simple and efficient methods for CO_2 sequestration is a significant environmental challenge. The CO_2 adsorption isotherms at 0 °C were measured for MCNS-900-5. A commercial activated carbon (AC) with S_{BET} = 1878 m^2/g and a micropore ratio of 83% (Figure S16) was selected as the control sample. MCNS-900-5 exhibited an adsorption capacity of 96 cm^3/g (i.e., 4.28 mmol/g), higher than that for AC (85 cm^3/g, Figure S17), although their S_{BET} values are close (Figure 4). This superior CO_2 capture performance could be attributed to the higher micropore ratio present in MCNS-900-5 than in AC (94% vs 83%), considering that micropores show stronger interaction with CO_2 than non-micropores, i.e., mesopores or macropores. In addition, the selectivity for CO_2 over N_2 for MCNS-900-5 was up to 9.9, implying a potentially attractive material for CO_2 separation.

The liquid-phase adsorption performance of these MCNSs was also explored in addition to gas-phase CO_2 adsorption properties. This potential application for MCNSs was evaluated by using methylene blue (MB) and vitamin B12 (VB12) as model adsorbates. MB has MW = 320 g/mol and molecular dimensions of 1.43 nm × 0.61 nm × 0.40 nm,[19] whereas VB12 has MW = 1355 g/mol and molecular dimensions of 1.84 nm × 1.41 nm × 1.14 nm (Table S6).[20] Figure 5A provides digital photos of the filtered solutions of MB and VB12 after exposure to MCNS-900-5 for various times. For the smaller-sized MB, the filtered solution turns from blue to colorless in 1.0 h, indicating rapid adsorption of MB in the MCNS-900-5. In contrast, for the larger-size VB12 molecules, the color of the filtered solution is almost constant, even after long adsorption times, e.g., 24.0 h, implying poor adsorption of VB12 into MCNS-900-5. Further quantitative measurements show that the saturation adsorption capacities of MB and VB12 on MCNS-900-5 are 292 and 21 mg/g, respectively (Figure 5B). These results clearly show that
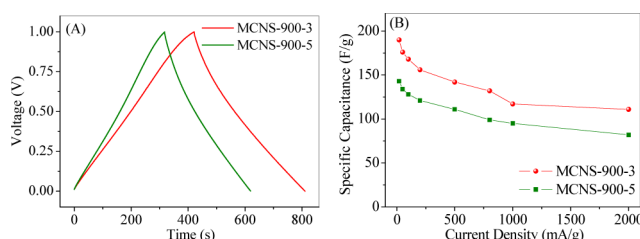
MCNS-900-5 demonstrates an excellent size-selective adsorption performance, since its micropores provide good accessibility for MB but not for VB12. In comparison, the control sample AC shows poor size-selective adsorption because of its broad pore size distribution. For instance, under the same measurement conditions, the saturation adsorption capacities of MB and VB12 on AC are 284 and 289 mg/g, respectively, indicating no adsorption selectivity (Figure S18).

Supercapacitors are among the most important clean energy storage devices due to their high power density, long cycle life, and short charging period.[21] MCNSs show high surface area, high microporosity, and well-defined spherical nanomorphology, which indicates they should be considered as candidates for supercapacitor electrodes. Furthermore, their well-developed micropores would interact strongly with electrolyte molecules, effectively enhancing the electrical double layer.[22] On the other hand, the uniform nanospherical morphology of MCNSs should decrease the ion diffusion distance, e.g., 165 nm radius of the nanospheres, which allows easy entry of the electrolytes into the inner micropores.[23] The electrochemical performance for MCNSs in both aqueous electrolyte of 6 M KOH and organic electrolyte of 1 M $(C_2H_5)_4NBF_4$/PC was characterized. The galvanostatic charge/discharge curves of MCNS-900-3 and MCNS-900-5 look nearly symmetric, and their cyclic voltammo-grams display a quasi-rectangular shape (Figures 6A and S19–S26). These results clearly confirm that MCNSs exhibit good electrochemical capacitive characteristics. For example, the specific capacitances of MCNS-900-3 at current densities of 20 and 2000 mA/g in 6 M KOH are 190 and 110 F/g, giving energy densities of 6.6 and 3.8 (W h)/kg, respectively (Figure 6B). Moreover, since the energy density is proportional to the square of the operation voltage, its energy storage capability can be greatly enhanced by replacing the aqueous electrolyte with 1 M $(C_2H_5)_4NBF_4$/PC, for example, achieving 113 F/g at 50 mA/g (Figure S27), indicative of a high energy density of 28.7 (W h)/kg, comparable to values for other carbon materials.[14d,24]

In conclusion, a simple yet versatile molecular-scale interface engineering concept has been developed for the design and fabrication of a novel class of well-defined MCNS materials, adopting the organic/inorganic hybrid molecule Ph-POSS as the building block for molecular-scale templating. Intra-/intermo-lecular cross-linking of the phenyl groups in a solution of Ph-POSS molecules causes phase separation, forming xPh-POSS nanosphere macroscopic particles. The resulting covalent polymeric/inorganic interface on the molecular scale is sufficiently stable to prevent the monodispersed Ph-POSS silica domains from thermal agglomeration when xPh-POSS is treated under proper carbonization conditions. This leads to well-defined carbon structures with silica-templated micropores of 1.3

Figure 5. (A) Photographs of MB and VB12 solutions with various times. (B) Adsorption curves of MB and VB12 for MCNS-900-5.

nm diameter, smaller than those present in other reported silica-templated porous carbons. The as-prepared MCNSs demonstrate high surface areas and high micropore ratios, in addition to retaining their valuable spherical nanomorphology. Thanks to these structural features, MCNSs exhibit good CO_2 capture and separation performances and excellent size-selective adsorption properties towards organic molecues, illustrated by highly selective adsorption of MB over VB12. The nanostructured carbons also perform well as supercapacitor electrodes with high capacitances. We hope that this molecular-scale interface engineering concept may lead to the development of more unique and unusual functional materials, and thus provide new opportunities in applications related to energy, adsorption, separation, catalysis, and medicine.

■ ASSOCIATED CONTENT

Ⓢ Supporting Information

Experimental details and characterization data. This material is available free of charge via the Internet at http://pubs.acs.org.

■ AUTHOR INFORMATION

Corresponding Author

wudc@mail.sysu.edu.cn; km3b@andrew.cmu.edu

Notes

The authors declare no competing financial interest.

■ ACKNOWLEDGMENTS

■ REFERENCES

(1) (a) Weng, Z.; Li, F.; Wang, D. W.; Wen, L.; Cheng, H. M. *Angew. Chem., Int. Ed.* **2013**, *52*, 3722. (b) Yang, S.; Bachman, R. E.; Feng, X.; Müllen, K. *Acc. Chem. Res.* **2013**, *46*, 116. (c) Wu, Z. S.; Sun, Y.; Tan, Y. Z.; Yang, S.; Feng, X.; Müllen, K. *J. Am. Chem. Soc.* **2012**, *134*, 19532.

(2) (a) Wu, Z. Y.; Li, C.; Liang, H. W.; Chen, J. F.; Yu, S. H. *Angew. Chem., Int. Ed.* **2013**, *52*, 2925. (b) Hao, G. P.; Li, W. C.; Qian, D.; Wang, G. H.; Zhang, W. P.; Zhang, T.; Wang, A. Q.; Schuth, F.; Bongard, H. J.; Lu, A. H. *J. Am. Chem. Soc.* **2011**, *133*, 11378.

(3) Chen, Z. P.; Ren, W. C.; Gao, L. B.; Liu, B. L.; Pei, S. F.; Cheng, H. M. *Nat. Mater.* **2011**, *10*, 424.

(4) Wu, Z. X.; Li, W.; Webley, P. A.; Zhao, D. Y. *Adv. Mater.* **2012**, *24*, 485.

(5) Raoof, M.; Cisneros, B. T.; Guven, A.; Phounsavath, S.; Corr, S. J.; Wilson, L. J.; Curley, S. A. *Biomaterials* **2013**, *34*, 1862.

(6) Nalwa, K. S.; Cai, Y. K.; Thoeming, A. L.; Shinar, J.; Shinar, R.; Chaudhary, S. *Adv. Mater.* **2010**, *22*, 4157.

(7) (a) Zhang, J.; Liu, X.; Blume, R.; Zhang, A. H.; Schlögl, R.; Su, D. S. *Science* **2008**, *322*, 73. (b) Zhang, P.; Gong, Y.; Li, H.; Chen, Z.; Wang, Y. *Nat. Commun.* **2013**, *4*, 1593. (c) Li, X.; Antonietti, M. *Chem. Soc. Rev.* **2013**, *42*, 6593. (d) Fellinger, T. P.; Hasché, F.; Strasser, P.; Antonietti, M. *J. Am. Chem. Soc.* **2012**, *134*, 4072.

(8) (a) Wu, D.; Xu, F.; Sun, B.; Fu, R.; He, H.; Matyjaszewski, K. *Chem. Rev.* **2012**, *112*, 3959. (b) McGann, J. P.; Zhong, M. J.; Kim, E. K.; Natesakhawat, S.; Jaroniec, M.; Whitacre, J. F.; Matyjaszewski, K.; Kowalewski, T. *Macromol. Chem. Phys.* **2012**, *213*, 1078. (c) Su, D. S.; Perathoner, S.; Centi, G. *Chem. Rev.* **2013**, *113*, 5782. (d) Xia, Y.; Yang,

Z.; Mokaya, R. *Nanoscale* **2010**, *2*, 639. (e) Fechler, N.; Fellinger, T. P.; Antonietti, M. *Adv. Mater.* **2013**, *25*, 75. (f) Presser, V.; Heon, M.; Gogotsi, Y. *Adv. Funct. Mater.* **2011**, *21*, 810.

(9) (a) Fang, Y.; Gu, D.; Zou, Y.; Wu, Z.; Li, F.; Che, R.; Deng, Y.; Tu, B.; Zhao, D. *Angew. Chem., Int. Ed.* **2010**, *49*, 7987. (b) Tang, C. B.; Tracz, A.; Kruk, M.; Zhang, R.; Smilgies, D. M.; Matyjaszewski, K.; Kowalewski, T. *J. Am. Chem. Soc.* **2005**, *127*, 6918. (c) Zhong, M.; Kim, E. K.; McGann, J. P.; Chun, S. E.; Whitacre, J. F.; Jaroniec, M.; Matyjaszewski, K.; Kowalewski, T. *J. Am. Chem. Soc.* **2012**, *134*, 14846. (d) Kruk, M.; Jaroniec, M.; Kim, T. W.; Ryoo, R. *Chem. Mater.* **2003**, *15*, 2815.

(10) (a) Lee, K. T.; Lytle, J. C.; Ergang, N. S.; Oh, S. M.; Stein, A. *Adv. Funct. Mater.* **2005**, *15*, 547. (b) Zhi, L. J.; Wu, J. S.; Li, J. X.; Kolb, U.; Müllen, K. *Angew. Chem., Int. Ed.* **2005**, *44*, 2120.

(11) (a) Liu, R.; Mahurin, S. M.; Li, C.; Unocic, R. R.; Idrobo, J. C.; Gao, H.; Pennycook, S. J.; Dai, S. *Angew. Chem., Int. Ed.* **2011**, *50*, 6799. (b) Lu, A. H.; Sun, T.; Li, W. C.; Sun, Q.; Han, F.; Liu, D. H.; Guo, Y. *Angew. Chem., Int. Ed.* **2011**, *50*, 11765.

(12) (a) Zou, C.; Wu, D.; Li, M.; Zeng, Q.; Xu, F.; Huang, Z.; Fu, R. *J. Mater. Chem.* **2010**, *20*, 731. (b) Wang, D. W.; Li, F.; Liu, M.; Lu, G. Q.; Cheng, H. M. *Angew. Chem., Int. Ed.* **2008**, *47*, 373. (c) Wu, D.; Hui, C. M.; Dong, H.; Pietrasik, J.; Ryu, H. J.; Li, Z.; Zhong, M.; He, H.; Kim, E. K.; Jaroniec, M.; Kowalewski, T.; Matyjaszewski, K. *Macromolecules* **2011**, *44*, 5846.

(13) (a) Liang, C.; Li, Z.; Dai, S. *Angew. Chem., Int. Ed.* **2008**, *47*, 3696. (b) Lu, A. H.; Schüth, F. *Adv. Mater.* **2006**, *18*, 1793. (c) Nishihara, H.; Kyotani, T. *Adv. Mater.* **2012**, *24*, 4473. (d) Yang, Z. X.; Xia, Y. D.; Mokaya, R. *J. Mater. Chem.* **2006**, *16*, 3417. (e) Matsuoka, K.; Yamagishi, Y.; Yamazaki, T.; Setoyama, N.; Tomita, A.; Kyotani, T. *Carbon* **2005**, *43*, 876. (f) Ariga, K.; Yamauchi, Y. *J. Mater. Chem. A* **2013**, *1*, 14.

(14) (a) Wan, Y.; Shi, Y. F.; Zhao, D. Y. *Chem. Mater.* **2008**, *20*, 932. (b) Fang, Y.; Lv, Y. Y.; Che, R. C.; Wu, H. Y.; Zhang, X. H.; Gu, D.; Zheng, G. F.; Zhao, D. Y. *J. Am. Chem. Soc.* **2013**, *135*, 1524. (c) Hu, Y. S.; Adelhelm, P.; Smarsly, B. M.; Hore, S.; Antonietti, M.; Maier, J. *Adv. Funct. Mater.* **2007**, *17*, 1873. (d) Jiang, H. L.; Liu, B.; Lan, Y. Q.; Kuratani, K.; Akita, T.; Shioyama, H.; Zong, F.; Xu, Q. *J. Am. Chem. Soc.* **2011**, *133*, 11854.

(15) (a) Han, B. H.; Zhou, W.; Sayari, A. *J. Am. Chem. Soc.* **2003**, *125*, 3444. (b) Wu, D.; Dong, H.; Pietrasik, J.; Kim, E. K.; Hui, C. M.; Zhong, M.; Jaroniec, M.; Kowalewski, T.; Matyjaszewski, K. *Chem. Mater.* **2011**, *23*, 2024. (c) Liang, Y. R.; Fu, R. W.; Wu, D. C. *ACS Nano* **2013**, *7*, 1748. (d) Liang, Y. R.; Lu, S. H.; Wu, D. C.; Sun, B.; Xu, F.; Fu, R. W. *J. Mater. Chem. A* **2013**, *1*, 3061.

(16) (a) Zheng, L.; Waddon, A. J.; Farris, R. J.; Coughlin, E. B. *Macromolecules* **2002**, *35*, 2375. (b) Zhang, W.; Müller, A. H. E. *Prog. Polym. Sci.* **2013**, *38*, 1121. (c) Liu, Y.; Shi, Z.; Xu, H.; Fang, J.; Ma, X.; Yin, J. *Macromolecules* **2010**, *43*, 6731.

(17) Li, Z. H.; Wu, D. C.; Liang, Y. R.; Xu, F.; Fu, R. W. *Nanoscale* **2013**, *5*, 10824.

(18) (a) Li, J. R.; Yu, J. M.; Lu, W. G.; Sun, L. B.; Sculley, J.; Balbuena, P. B.; Zhou, H. C. *Nat. Commun.* **2013**, *4*, 1538. (b) Zhong, M. J.; Natesakhawat, S.; Baltrus, J. P.; Luebke, D.; Nulwala, H.; Matyjaszewski, K.; Kowalewski, T. *Chem. Commun.* **2012**, *48*, 11516.

(19) Liu, Q.-S.; Zheng, T.; Li, N.; Wang, P.; Abulikemu, G. *Appl. Surf. Sci.* **2010**, *256*, 3309.

(20) Tamai, H.; Kakii, T.; Hirota, Y.; Kumamoto, T.; Yasuda, H. *Chem. Mater.* **1996**, *8*, 454.

(21) (a) Kou, Y.; Xu, Y. H.; Guo, Z. Q.; Jiang, D. L. *Angew. Chem., Int. Ed.* **2011**, *50*, 8753. (b) Su, D. S.; Schlögl, R. *ChemSusChem* **2010**, *3*, 136.

(22) Chmiola, J.; Yushin, G.; Gogotsi, Y.; Portet, C.; Simon, P.; Taberna, P. L. *Science* **2006**, *313*, 1760.

(23) Xu, F.; Cai, R. J.; Zeng, Q. C.; Zou, C.; Wu, D. C.; Li, F.; Lu, X. E.; Liang, Y. R.; Fu, R. W. *J. Mater. Chem.* **2011**, *21*, 1970.

(24) (a) Zhao, X.; Wang, A.; Yan, J.; Sun, G.; Sun, L.; Zhang, T. *Chem. Mater.* **2010**, *22*, 5463. (b) Centenoa, T. A.; Stoeckli, F. *Electrochem. Commun.* **2012**, *16*, 34.